Alignment of defect levels and band edges through hybrid functionals: Effect of screening in the exchange term

Hannu-Pekka Komsa,* Peter Broqvist, and Alfredo Pasquarello
Institute of Theoretical Physics, Ecole Polytechnique Fédérale de Lausanne (EPFL), CH-1015 Lausanne, Switzerland and Institut Romand de Recherche Numérique en Physique des Matériaux (IRRMA), CH-1015 Lausanne, Switzerland
(Received 21 January 2010; revised manuscript received 28 April 2010; published 21 May 2010)

We investigate how various treatments of exact exchange affect defect charge transition levels and band edges in hybrid functional schemes for a variety of systems. We distinguish the effects of long-range vs short-range exchange and of local vs nonlocal exchange. This is achieved by the consideration of a set of four functionals, which comprise the semilocal Perdew-Burke-Ernzerhof (PBE) functional, the PBE hybrid (PBE0), the Heyd-Scuseria-Ernzerhof (HSE) functional, and a hybrid derived from PBE0 in which the Coulomb kernel in the exact exchange term is screened as in the HSE functional but which, unlike HSE, does not include a local expression compensating for the loss of the long-range exchange. We find that defect levels in PBE0 and in HSE almost coincide when aligned with respect to a common reference potential, due to the close total-energy differences in the two schemes. At variance, the HSE band edges determined within the same alignment scheme are found to shift significantly with respect to the PBE0 ones: the occupied and the unoccupied states undergo shifts of about +0.4 eV and −0.4 eV, respectively. These shifts are found to vary little among the materials considered. Through a rationale based on the behavior of local and nonlocal long-range exchange, this conclusion is generalized beyond the class of materials used in this study. Finally, we explicitly address the practice of tuning the band gap by adapting the fraction of exact exchange incorporated in the functional. When PBE0-like and HSE-like functionals are tuned to yield identical band gaps, their respective results for the positions of defect levels within the band gap and for the band alignments at interfaces are found to be very close.

DOI: 10.1103/PhysRevB.81.205118 PACS number(s): 71.15.−m, 71.55.−i

I. INTRODUCTION

Hybrid functionals are orbital-dependent functionals in which the exchange term is described partly by exact nonlocal exchange and partly by a semilocal expression.[1,2] Calculations for a standard set of molecules show that hybrid functionals give total energies of a higher accuracy than (semi)local-density functionals, such as the local-density approximation or the generalized gradient approximation.[3] While hybrid functionals have rapidly grown into a standard tool in quantum chemistry, their general use in condensed-matter electronic-structure research is much more recent and has long been hampered by the high computational cost associated to the treatment of nonlocal exchange in plane-wave basis sets. At present, it appears that a transition from gradient-corrected density functionals to hybrid functionals is taking place, resembling very much the one in the mid-nineties from purely local density functionals to gradient-corrected density functionals.[4,5]

With respect to semilocal functionals, hybrid functionals give an improved description of several properties, such as formation enthalpies, bond lengths of molecules, lattice parameters, bulk moduli, etc.[3,6–10] However, their ability[11–15] of yielding band gaps and excitation energies in generally better agreement with experiment has often been one major motivation for adopting this new paradigm. Indeed, electronic-structure research involving the positioning of defect levels with respect to relevant band edges[16–28] and the band alignment at interfaces[29,30] have already been taking advantage of such hybrid functional schemes.

There exists a variety of hybrid functionals that are presently in use. In condensed-matter electronic-structure research, the most popular hybrid functionals are derived from the generalized gradient approximation proposed by Perdew, Burke, and Ernzerhof (PBE).[31] A class of hybrid functionals is derived therefrom by replacing a fraction of PBE exchange by its nonlocal counterpart.[32] A general rationale has been developed favoring a fraction of 25%, although other fractions might admittedly be more appropriate for specific materials or even properties. The hybrid functional with a fraction of 25% is here referred to as PBE0[32] but other denominations such as PBE1PBE (Ref. 7) and PBEh are also in use.

More recently, Heyd, Scuseria, and Ernzerhof (HSE) introduced a hybrid functional in which the fraction of nonlocal exchange is preserved at short range but replaced by a semilocal expression at long range.[8,33] The separation between short-range and long-range exchange is achieved through the replacement of the Coulomb potential by a screened potential in the nonlocal exchange part, in the spirit of the screened exchange method used within the local-density approximation (sX-LDA).[34] The HSE functional thereby removes some unphysical features of exact nonlocal exchange in the description of metallic systems.[8] Furthermore, the HSE functional offers computational advantages in converging the long-range exchange contribution in both Gaussian and plane-wave formulations.[8,13]

In this work, we systematically investigate how the various treatments of exchange in hybrid functionals affect (i) the relative location of calculated defect levels and band edges and (ii) the calculated band alignment at interfaces. We focus on hybrid functionals that are currently in use in the literature such as the PBE0 and HSE functionals, and distin-

guish the effects of long-range vs short-range exchange and of local vs nonlocal exchange. In our study, we also address the common practice of tuning the fraction of exact exchange to match the electronic band gap. For illustrating these effects, we consider a set of semiconductors and insulators covering a wide range of band gaps. Our calculations reveal that the energy levels obtained with these functionals show characteristic shifts which are to a large extent material independent. We provide a rationale which generalizes this conclusion beyond the class of materials used in this study.

Our paper is organized as follows. In Sec. II, we describe the class of functionals used in this work. We also give in this section a description of the physical quantities considered in this work. In Sec. III, we focus on total-energy differences associated to localized systems, such as ionization potentials of molecular systems and charge transition levels of point defects in extended bulk systems. Section IV is devoted to delocalized states. More specifically we focus on the energy levels of the band edges of extended bulk materials and on the band alignment at interfaces between two materials. In Sec. V, we provide a rationale for understanding our results. The conclusions are drawn in Sec. VI.

II. FUNCTIONALS

In this paper, we use four functionals which differ by the way the exchange energy is treated. This approach enables us to examine step-by-step how different treatments of the exchange energy affect the results. In all functionals adopted in this work, the correlation energy corresponds to that used in the generalized gradient approximation proposed by Perdew, Burke, and Ernzerhof.[31]

The first functional corresponds to the standard PBE functional. Thus, the exchange energy is given by the purely semilocal PBE exchange E_x^{PBE}.[31]

The second functional corresponds to the PBE0 hybrid[32] in which 25% of PBE exchange is replaced by exact nonlocal exchange showing the normal $1/r$ kernel. When α is allowed to vary, we refer to the generalized class of functionals given by

$$E_x^{\mathrm{PBE0}}(\alpha) = \alpha E_x^{\mathrm{exact}} + (1-\alpha)E_x^{\mathrm{PBE}}. \tag{1}$$

The third functional is the HSE screened hybrid.[8,33] The HSE functional is derived from PBE0 by replacing the long-range part of the exact exchange by a local expression of PBE exchange. Or, alternatively, the HSE functional is derived from PBE by replacing a fraction of short-range local PBE exchange by corresponding exact short-range exchange. The separation between short-range and long-range exchange is achieved through the use of a screened exchange kernel given by $\mathrm{erfc}(\omega r)/r$, where the parameter ω corresponds to an inverse screening length and defines the extent of the exchange kernel in real space. The original HSE functional, referred to HSE06 in the literature, carries the parameters α=25% and ω=0.106 bohr^{-1}.[33] For generic parameters α and ω,

$$E_x^{\mathrm{HSE}}(\alpha,\omega) = \alpha E_x^{\mathrm{exact,SR}}(\omega) + (1-\alpha)E_x^{\mathrm{PBE,SR}}(\omega) + E_x^{\mathrm{PBE,LR}}(\omega). \tag{2}$$

The fourth functional, which we refer to as sPBE0, is derived from PBE0 by introducing a screened kernel in the part of exact exchange,

$$E_x^{\mathrm{sPBE0}}(\alpha) = \alpha E_x^{\mathrm{exact,SR}} + (1-\alpha)E_x^{\mathrm{PBE}}. \tag{3}$$

The screening is described in the same way as in the short-range part of the HSE functional. However, unlike the HSE functional, the missing long-range exchange is not restored by a local expression. For α and ω, we use the same values as in HSE. This kind of functional in which the long-range exchange associated to the screened kernel is completely missing, has already been used in the literature.[20,21,30,35]

The first three functionals can all be described through the HSE-like functional given in Eq. (2) by setting specific values for the parameters α and ω. Furthermore, the following relationships hold: (i) all hybrid functionals transform to PBE for $\alpha \to 0$; (ii) HSE and sPBE0 become equivalent to PBE0 for $\omega \to 0$; and (iii) HSE is identical to PBE in the limit $\omega \to \infty$.

While we do not explicitly treat sX-LDA functionals in this work, it is worth pointing out that sX-LDA and HSE are conceptually similar. Both sX-LDA and HSE rely on a screened Coulomb kernel in the exact exchange term. Both sX-LDA and HSE involve a separation of short-range and long-range exchange and both replace the nonlocal long-range exchange by a semilocal expression. However, the semilocal reference for sX-LDA is the local-density approximation, instead of the PBE adopted in HSE. In sX-LDA, 100% of the short-range exchange is calculated exactly compared to only 25% in HSE. The most significant difference concerns the screening length: sX-LDA adopts a Thomas-Fermi screening length which depends on the electron density while the screening length is a fixed parameter in HSE. When the used screening lengths are close, the present discussion involving HSE should similarly apply to sX-LDA.

Defect energy levels are determined through the standard formation energy formulation based on total-energy differences.[36] The formation energy of a defect in the charge state q is derived as a function of the electron chemical potential μ,

$$E_f^q(\mu) = E_{\mathrm{tot}}^q - E_{\mathrm{tot}}^{\mathrm{bulk}} - \sum_i n_i\eta_i + q(\mu + \varepsilon_v + \Delta V) + E_{\mathrm{corr}}^q, \tag{4}$$

where E_{tot}^q and $E_{\mathrm{tot}}^{\mathrm{bulk}}$ are the calculated total energies of the defect and the host supercells, n_i and η_i are the number and the chemical potential of the added (or removed) atomic species, and $\varepsilon_v+\Delta V$ corresponds to the bulk valence-band maximum in the energy reference of the defect calculation. E_{corr}^q takes care of the spurious electrostatic interactions due to periodicity. Here, we only included the first order monopole corrections,[37] which generally produces improved results for both molecules and defects. We note that this correction is the same for all functionals, and therefore does not affect the comparison between the functionals.

The charge transition levels correspond to electron chemical potentials for which the formation energies of two different charge states are equal,

$$\mu_{q/q'} = \frac{(E_{\rm tot}^{q'} - E_{\rm tot}^{q}) + (E_{\rm corr}^{q'} - E_{\rm corr}^{q})}{q - q'} - \varepsilon_v - \Delta V. \qquad (5)$$

For convenience, we also define the charge transition levels $\bar{\mu}_{q/q'}$ with respect to the average electrostatic potential ϕ through the relation $\bar{\mu}_{q/q'} = \mu_{q/q'} - \phi$.

In order to highlight electronic-structure effects associated to the exchange term, the calculations with the various functionals were performed for the same structural geometries, for which we took the equilibrium structures at the PBE level. All the calculations were performed within a scheme based on plane-wave basis sets and normconserving pseudopotentials. The pseudopotentials were generated at the PBE level and used without modification with all the functionals. Comparisons with all-electron calculations indicate that such a pseudopotential approach can be very accurate when the charge densities of core and valence wave functions do not show significant overlap.[38] We used an energy cutoff of 70 Ry, unless specified otherwise. The reciprocal-space sampling is generally performed using the sole Γ point. For the materials and supercell sizes considered in this work, this leads to converged results in all cases except for bulk silicon[38] in which case a finer sampling was used. All the calculations involving nonlocal exchange, either screened or unscreened, include a singularity correction to accelerate the convergence with k-point sampling in reciprocal space.[38] This also guarantees that the screened functionals correctly approach the PBE0 results in the limit $\omega \to 0$.

The calculations were performed with the codes QUANTUM-ESPRESSO (Ref. 39) and CPMD.[40] For the purpose of this project, we implemented the HSE subroutines[41] in both codes. In the implementation, the long-range exchange energy $E_x^{\rm PBE,LR}$ in Eq. (2) is obtained through the expression, $E_x^{\rm PBE,LR} = E_x^{\rm PBE} - E_x^{\rm PBE,SR}$, in which the PBE exchange explicitly appears. The derivation of the $E_x^{\rm PBE,SR}$ term is based on the exchange hole formulation of the PBE functional.[42] For internal consistency, the original HSE functional thus uses this formulation. However, the results obtained with the exchange-hole PBE functional barely differ from those obtained with the conventional PBE functional. For instance, we found variations in the eigenvalues of silicon within 20 meV. Hence, we chose to use the conventional PBE functional in the present work in order to exactly recover the PBE limit for $\alpha \to 0$.

III. LOCALIZED STATES

A. Finite systems

Comparisons between the performances of PBE0 and HSE for molecular properties based on total-energy differences, such as formation enthalpies, have already been presented in the literature.[8,43] The results are generally very similar insofar the screening length often exceeds the size of the molecule. However, the (generalized) Kohn-Sham eigenvalues are seldom reported.

Here, we study two molecules in detail: the nitrogen dimer (N_2) and naphthalene ($C_{10}H_8$). For both molecules, we used cubic simulation cells with sides of 30 bohrs. The energy cutoff was set to 90 Ry for N_2 and to 70 Ry for naphthalene. The calculated results are given in Table I and include the Kohn-Sham eigenvalues of the highest occupied molecular orbital (HOMO) and of the lowest unoccupied molecular orbital (LUMO) referenced with respect to the vacuum level, the corresponding Kohn-Sham energy gap, and the ionization potentials (IPs) derived from total-energy differences.

TABLE I. The (generalized) Kohn-Sham eigenvalues of the highest occupied molecular orbital (HOMO) and of the lowest unoccupied molecular orbital (LUMO) levels referenced with respect to the vacuum level, the corresponding Kohn-Sham energy gaps ($E_g^{\rm KS}$), and the ionization potentials (IP) calculated with various functionals for the N_2 dimer and the naphthalene molecule. All energies are in electron volt. Experimental values are from Ref. 44.

	HOMO	LUMO	$E_g^{\rm KS}$	IP
N_2				
PBE	−10.25	−1.95	8.30	15.29
PBE0	−12.16	−0.64	11.52	15.67
HSE	−11.76	−1.02	10.74	15.66
sPBE0	−11.36	−0.64	10.73	15.26
Expt.				15.58
Naphthalene				
PBE	−5.51	−2.12	3.39	7.96
PBE0	−6.39	−1.33	5.06	8.06
HSE	−6.00	−1.69	4.32	8.05
sPBE0	−5.62	−1.31	4.32	7.67
Expt.				8.14

The ionization potentials calculated in the PBE are already fairly close to the experimental values. The PBE0 and HSE results are very close to each other and improve over the PBE results. The close agreement achieved between the sPBE0 and PBE results for N_2 appears accidental since such a matching is not found for naphthalene.

The LUMO levels are very close in PBE0 and sPBE0. At variance, with respect to PBE0, the LUMO levels found in HSE drop by 0.38 eV and 0.36 eV for N_2 and naphthalene, respectively. Shifts of similar size are also found for the HOMO. For both molecules, the HOMO level in HSE is about 0.4 eV higher than in PBE0 while the HOMO level in sPBE0 is about 0.8 eV higher than in PBE0. Consequently, the Kohn-Sham energy gap in HSE and sPBE0 are very close, underestimating the PBE0 energy gap by 0.7–0.8 eV. The fact that the energy gaps in HSE and sPBE0 are close should be assigned to the occurrence of the same nonlocal exchange term in both functionals, leading to the same band-gap opening in the generalized Kohn-Sham eigenvalue spectrum.[45] With respect to sPBE0, HSE also includes the effect of the long-range PBE exchange, which by comparison is found to shift the eigenvalues of occupied and unoccupied states downward by about 0.4 eV.

For the specific case of the N_2 dimer, we determined the equilibrium bond length for each functional. We found bond lengths of 1.102 Å (PBE), 1.090 Å (PBE0), 1.090 Å

(HSE), and 1.092 Å (sPBE0). These results compare very well with projector-augmented-wave and all-electron results reported in Ref. 43, conferring further confidence to our pseudopotential results. Moreover, since the N_2 bond length is very similar for all hybrid functionals, the above discussion about eigenvalue shifts holds in this case also for relaxed geometries.

B. Defects

In a recent investigation,[22] it was shown that charge transition levels of atomic-size defects do not significantly change when going from PBE to PBE0, provided the defect levels are aligned with respect to a common reference potential. We here extend the comparison to sPBE0 and HSE.

The correspondence between defect levels appears quite robust but deteriorates when the extension of the defect wave function increases[22] or when its character closely resembles that of the bulk band states.[26] Therefore, we here focus on α-quartz SiO_2 for which the identified trends appear most clearly because of its large band gap. Following Ref. 22, we modeled SiO_2 with a bulk model of 72 atoms and considered a set of 17 transition levels for five different types of defects. More specifically, we considered the following defects and charge states: the interstitial H (+1,0,−1), the H bridge -Si-H-Si- (+1,0,−1), the Si dimer (+1,0), the interstitial O_2 (0,−1), and the substitutional N (0,−1). Both thermodynamic and vertical charge transition levels were calculated. For the alignment, we took the average electrostatic potential. In Fig. 1, the transition levels determined within sPBE0 and HSE are displayed vs the PBE0 results. The HSE results are found to agree well with the PBE0 results, and consequently also with the PBE results.[22] At variance, the sPBE0 results appear to be rigidly shifted upward by 0.41 eV with respect to PBE0 (and thus also to HSE and PBE).

These results indicate that the defect levels obtained with either PBE0-like or HSE-like functionals do not shift significantly when the fraction of exact exchange varies between α=0% and α=25%. A more detailed analysis shows that the small shifts depend linearly on α (Ref. 24) because of the linear nature of the mixing and the negligible variations undergone by the wave functions.[46]

We also investigated how defect levels are affected when the screening parameter ω is varied within the functional form of the HSE functional. We focus on the substitutional nitrogen defect in α-quartz SiO_2. In Fig. 2, we give the evolution of the thermodynamic (0/−1) charge transition level for ω varying between 0 and 0.2 $bohr^{-1}$. For this range of values, we found the defect level to shift by about 35 meV, which is negligible with respect to the shifts undergone by the SiO_2 band edges (Fig. 2). Figure 2 also shows the detailed evolution of the defect level with ω, exhibiting a nonlinear behavior at small ω.

IV. DELOCALIZED STATES

A. Band edges

In this section, we compare how the (generalized) Kohn-Sham eigenvalues pertaining to the band edges shift for the four functionals used in this work. Since the PBE0 and HSE defect levels do not undergo significant shifts, their position in the band gap is directly determined by the band-edge shifts.

We considered four bulk materials with band gaps ranging from 1.1 to 9 eV: silicon, 4H-SiC, monoclinic HfO_2, and

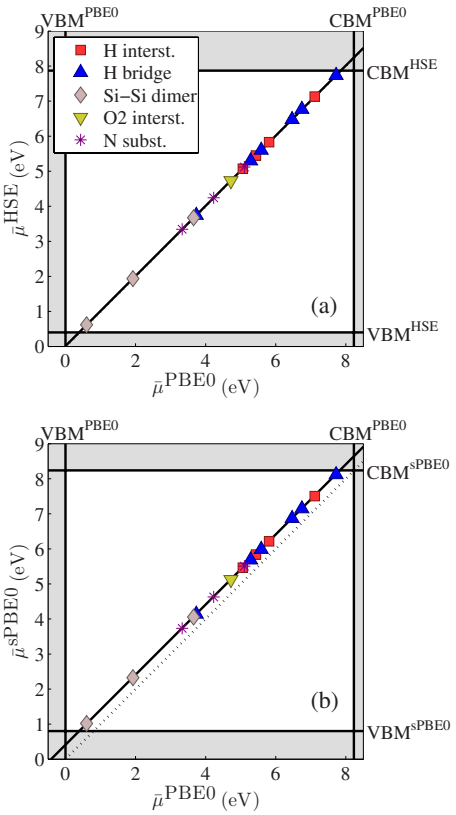

FIG. 1. (Color online) Comparison of the charge transition levels in α-quartz SiO_2: (a) HSE vs PBE0 and (b) sPBE0 vs PBE0. The solid lines are obtained through linear regressions whereas the dotted line in (b) indicates the ideal correspondence. All energies are referred to the average electrostatic potential, shifted to coincide with the PBE0 valence-band maximum for convenience.

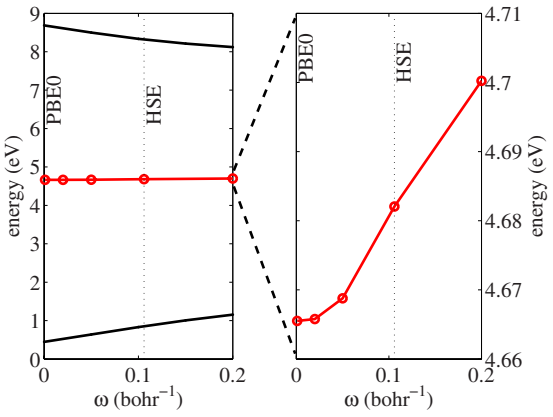

FIG. 2. (Color online) The (0/−) charge transition level $\bar{\mu}$ of substitutional nitrogen and the bulk band edges in α-quartz SiO_2 determined with the functional form of HSE for varying screening parameter ω. The results corresponding to the PBE0 and HSE functionals are recovered for ω=0 and ω=0.106 $bohr^{-1}$, respectively.

α-quartz SiO_2. For silicon, we used a primitive cell with a Γ-centered $12\times12\times12$ **k**-point sampling. The Brillouin-zone integration in the matrix elements of the exchange operator is performed with a coarser $6\times6\times6$ (**q**-point) mesh.[13] The PBE-optimized lattice constant is 5.465 Å, only slightly larger than the experimental value (5.43 Å, Ref. 47). For 4H-SiC, we used a 96-atom supercell and relaxed the atomic coordinates while keeping the c/a ratio fixed at the experimental value of 3.2714 (Ref. 48). This resulted in a lattice constant of 3.096 Å,[30] in good agreement with the experimental value of 3.073 Å. For monoclinic HfO_2, we used a 96-atom $2\times2\times2$ supercell with PBE cell parameters $a=5.09$ Å, $b=5.12$ Å, $c=5.34$ Å, and $\beta=99.61°$.[20] Corresponding experimental values are $a=5.12$ Å, $b=5.17$ Å, and $c=5.29$ Å, and $\beta=99.11°$.[49] For α-quartz SiO_2, we used a 72-atom supercell with $a=4.97$ Å and $c=5.45$ Å, to be compared with the corresponding experimental values of $a=4.91$ Å and $c=5.40$ Å.[50]

The band-edge positions expressed as shifts with respect to the PBE values are collected for all hybrid functionals in Table II. Different calculations are aligned through the average electrostatic potential. The generalized Kohn-Sham values obtained with the various hybrid functionals follow the same trends found for the molecules. The conduction band edges obtained with PBE0 and sPBE0 are very close, the band gaps obtained with HSE and sPBE0 are very close, and the valence-band edges shift upward by ~0.4 eV when going from PBE0 to HSE and by ~0.8 eV when going from PBE0 to sPBE0. Consequently, there appears to be a material-independent shift of ~0.8 eV in the band gap when going from PBE0 to HSE or sPBE0. Band-gap differences of similar size between PBE0 and HSE have been obtained previously[9] but a clear trend could not be revealed because of the use of relaxed (and thus different) structures. A rationale for the origin of these shifts will be provided in Sec. V.

We could not identify any material-independent relation between the band edges obtained with the PBE functional and those obtained with PBE0 and HSE hybrid functionals. For the present set of investigated materials, about 60–70 % of the band gap increase results from a downwards shift of the valence band. However, this trend does not appear to be general since in the case of germanium, the conduction-band shift has been found to dominate.[24]

For specific choices of the parameters α and ω, the functionals PBE, PBE0, and HSE can be obtained from the HSE-like functional given in Eq. (2). We illustrate this relationship by studying in Fig. 3 the band gap of α-quartz SiO_2 in the two-dimensional parameter space defined by α and ω. Varying α at fixed ω corresponds to moving along vertical lines. The most common functionals are achieved for $\omega=0$ and $\omega=0.106$ bohr^{-1}, corresponding to PBE0-like and HSE-like functionals, respectively. For PBE0-like functionals, the band gap increases linearly with the fraction α, in accord with previous investigations.[24,29] Figure 3 shows that the linear increase in the band gap with α approximately also holds for HSE-like functionals, albeit with a smaller rate. In case one wants the calculation to achieve a band gap of 9.3 eV, this can be realized either by setting $\alpha\approx35\%$ in PBE0-like functionals or $\alpha\approx50\%$ in HSE-like functionals. Going further to even smaller screening lengths, and therefore larger ω, this would require a very large fraction of exact exchange reaching ultimately the limit of $\alpha=100\%$, as in the sX-LDA method. However, for such large values of ω, it has been observed that the thermochemistry of molecular systems degrades.[8,51] As far as the dependence on ω at fixed α is concerned (horizontal axes in Fig. 3), we observe a stronger nonlinearity, particularly for $\omega>0.106$ bohr^{-1}.

In the latest generation of nonscreened hybrid functionals, the fraction of exact exchange α is the only remaining parameter.[32] Its value is generally fixed to 25% as done in PBE0 but may admittedly be material or even property dependent.[32] It has thus become common practice tuning the parameter α of PBE0-like and HSE-like functionals in order to reproduce the experimental band gap. It is therefore of interest to determine whether different hybrid functionals yield defect levels at similar locations within the band gap. Since it has been found that scaling α does not significantly affect the positions of defect levels when aligned with respect to the average electrostatic potential (cf. Ref. 22 for PBE0 and Sec. III B for HSE), the location within the band

TABLE II. (Generalized) Kohn-Sham eigenvalues for valence (ΔE_v) and conduction (ΔE_c) band edges of Si, α-quartz SiO_2, 4H-SiC, and monoclinic HfO_2, calculated with various hybrid functionals. The eigenvalues are expressed as shifts with respect to the PBE values and different calculations are aligned through the average electrostatic potential. Band gaps (E_g) and corresponding band gap variations (ΔE_g) are also given. The shifts of valence- and conduction-band edges are also expressed relative to the band-gap variation: $\Delta E_v^{rel}=\Delta E_v/\Delta E_g$, $\Delta E_c^{rel}=\Delta E_c/\Delta E_g$. All energies are in electron volt.

	E_g	ΔE_v	ΔE_c	ΔE_g	ΔE_v^{rel}	ΔE_c^{rel}
Si						
PBE	0.61					
PBE0	1.85	−0.70	0.54	1.24	56.3%	43.7%
HSE	1.20	−0.37	0.22	0.58	62.7%	37.1%
sPBE0	1.17	0.03	0.59	0.56	−4.8%	104.9%
SiC						
PBE	2.23					
PBE0	3.95	−1.03	0.70	1.72	59.5%	40.5%
HSE	3.18	−0.63	0.32	0.95	66.1%	33.9%
sPBE0	3.17	−0.23	0.71	0.94	24.7%	75.3%
HfO_2						
PBE	4.34					
PBE0	6.75	−1.49	0.92	2.41	61.7%	38.3%
HSE	5.98	−1.09	0.55	1.64	66.5%	33.5%
sPBE0	5.96	−0.69	0.93	1.62	42.5%	57.5%
SiO_2						
PBE	5.64					
PBE0	8.23	−1.75	0.84	2.59	67.6%	32.4%
HSE	7.47	−1.35	0.48	1.82	73.9%	26.1%
sPBE0	7.44	−0.95	0.85	1.79	52.8%	47.2%

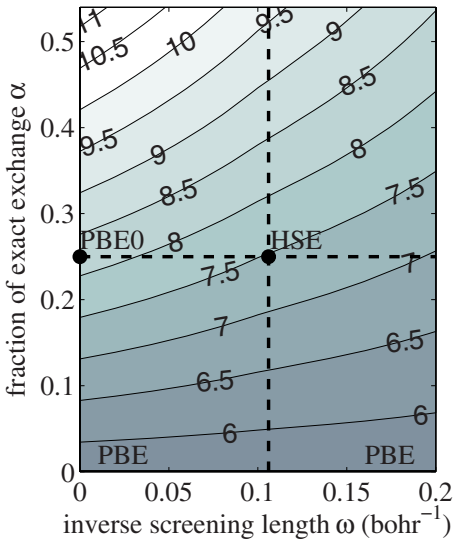

FIG. 3. (Color online) Band gap of α-quartz SiO_2 calculated with the HSE-like functional for varying parameters α and ω. The results corresponding to PBE0 and HSE are indicated by black disks. The PBE band gap is found in correspondence of the axis $\alpha=0$.

gap ultimately depends on the position of the band edges. In Table III, we give the position of the valence-band edges for the four bulk materials studied in this section when calculated with PBE0-like and HSE-like functionals in which the parameter α has been tuned. As illustrated in Fig. 4 for α-quartz SiO_2, this procedure results in different values of α for PBE0-like and HSE-like functionals but yields in both cases identical band gaps tuned to a desired value. The band structures found with α-tuned PBE0-like and HSE-like functionals do not coincide and their displacement shows a tendency to increasing with band gap (Table III). However, the observed shifts are relatively small reaching a value of just $\sim$0.2 eV in the worst case corresponding to SiO_2, for which the largest values of α are required. This implies that, for the materials studied, the locations of defect levels within the band gap as found with tuned PBE0-like and HSE-like hybrid functionals agree rather closely.

TABLE III. Valence-band position (ΔE_v) for functionals in which the fraction of exact exchange is tuned (α^{opt}) to reproduce the desired band gap (E_g^{opt}), for PBE0-like and HSE-like functionals. The band-edge energies are expressed as shifts with respect to the PBE values and different calculations are aligned through the average electrostatic potential. The last column gives the difference between the valence-band positions achieved with the two types of hybrid functionals. All energies are in electron volt.

		PBE0		HSE		
	E_g^{opt}	α^{opt}	ΔE_v	α^{opt}	ΔE_v	Diff.
Si	1.2	0.11	−0.31	0.23	−0.34	−0.03
SiC	3.3	0.15	−0.62	0.27	−0.68	−0.07
HfO_2	5.8	0.15	−0.89	0.22	−0.96	−0.07
SiO_2	9.3	0.35	−2.45	0.50	−2.68	−0.23

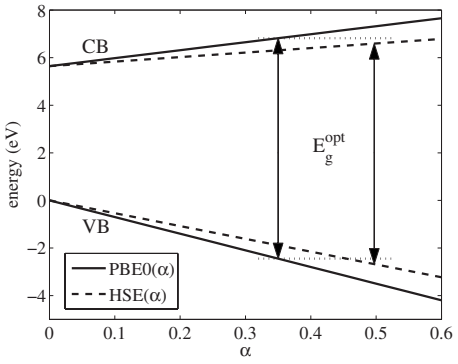

FIG. 4. Band-edge shifts of α-quartz SiO_2 vs the fraction of exact exchange α for PBE0-like and HSE-like functionals. The achievement of a given value for the band gap E_g^{opt}=9.3 eV is indicated for the two types of functionals and is achieved in correspondence of very close energy levels for the band edges. The energies are aligned with respect to the average electrostatic potential.

The differences between the band edges obtained with α-tuned HSE and PBE0 functionals are related to the ratio between the contributions of conduction- and valence-band shifts to the band gap opening. In PBE0-like functionals, this ratio is governed by the exact exchange term, generally leading to unequal displacements of occupied and unoccupied states. When the HSE eigenvalues are compared to the PBE0 ones, we noticed a symmetric closing of the calculated band gap by an upward shift of the valence band and a downward shift of the conduction band, the size of these shifts scaling linearly with α. Therefore, the eigenvalue differences between PBE0-like and HSE-like functionals cannot be eliminated by scaling the fraction α, unless the exchange-induced valence and conduction band shifts are equal. Hence, the observation that the α-tuned HSE eigenvalues given in Table III lie systematically lower than the α-tuned PBE0 ones is a direct consequence of the dominating valence band shift for the materials studied (cf. Table II).

B. Band offsets

Band offsets at interfaces are directly affected by shifts of band edges, and furthermore allow for direct comparisons with experiment. To access band offsets, we rely on a procedure which consists in determining the lineup of the local electrostatic potential across an interface model.[52] The band offsets are then found by aligning the band structures of the two bulk components to the potential on either side of the interface.

We first focus on the lineup of the electrostatic potential as found for various functionals. For illustration, we adopt an atomistic model interface of the Si-SiO_2 interface comprising 217 atoms in a superlattice geometry.[53] As bulk model for amorphous SiO_2, we took an atomistic structure generated by *ab initio* molecular dynamics.[54] We determined the planar-averaged electrostatic potential as a function of the coordinate z across the interface in the PBE, PBE0, HSE, and sPBE0. In Fig. 5, we display the difference between the PBE and PBE0 potentials, which indicates an alteration of the potential lineup by 0.16 eV. This result was first obtained in

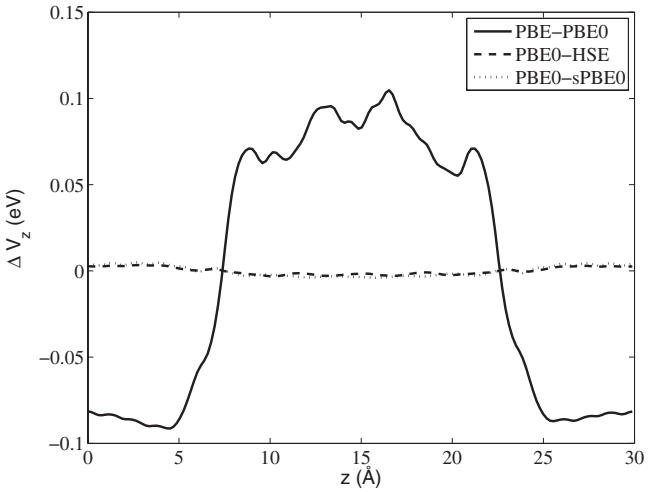

FIG. 5. Differences between planar-averaged electrostatic potentials across the Si-SiO_2 interface, when going from PBE to PBE0, from PBE0 to HSE, and from PBE0 to sPBE0.

Ref. 29, where it was also found that this offset scales linearly with α. We here extend this analysis to HSE and sPBE0 functionals. Figure 5 shows that the potential offset varies by only about 5 meV, when going from PBE0 to HSE or from PBE0 to sPBE0. These results generalize the notion that the offsets due to the electrostatic dipoles are not affected in a significant way by the use of hybrid functionals.[29] Similar results were also obtained for surface calculations.[55] The insensitivity of interface (or surface) dipoles to the adopted (hybrid) density functional also confers physical meaning to the alignment through the average electrostatic potential adopted throughout this work.[22] Indeed, under the assumption of an invariant charge density, this alignment would be *exactly* equivalent to that through an external vacuum level. A detailed discussion about this point is given in Ref. 56.

To obtain the band offsets, the second aspect that needs to be considered concerns the alignment of the band edges with respect to the local average potential on either side of the interface. This precisely corresponds to the valence-band shifts discussed in Sec. IV B (cf. Table III). When going from PBE to a hybrid functional, the major effect results from shifts of the band edges such as those calculated in Table II since we have seen that electrostatic effects are much weaker. For the Si-SiO_2 interface, the band offsets calculated with the various functionals are given in Table IV. The hybrid functional results clearly differ from the PBE one.[29] However, the different hybrid functionals used in this work all yield essentially the same band offsets.

The behavior of the band offsets calculated with the various hybrid functionals can be inferred from the behavior of the generalized Kohn-Sham eigenvalues. Assuming that the observed shifts of the valence-band edges by +0.4 eV (+0.8 eV) between HSE (sPBE0) and PBE0 are indeed material-independent (see Sec. V), we conclude that the band offsets calculated in PBE0, HSE, and sPBE0 are generally very close. This conclusion is indeed also consistent with earlier results for the band offsets at the SiC-SiO_2 interface, which showed identical values for PBE0 and sPBE0.[30]

While band offsets determined with hybrid functional schemes generally improve upon the semilocal PBE scheme,

TABLE IV. Valence-band offsets (VBOs) and conduction-band offsets (CBOs) calculated for the Si-SiO_2 interface with various hybrid functionals. Results obtained with the mixed scheme proposed in Ref. 29 are also shown. The corresponding band gaps E_g for silicon and amorphous SiO_2 (a-SiO_2) are given. Experimental results for the band offsets are from Ref. 57. Energies are in electron volt.

	E_g(Si)	E_g(a-SiO_2)	VBO	CBO
PBE	0.6	5.3	2.5	2.2
PBE0	1.8	7.9	3.2	2.8
HSE	1.2	7.1	3.2	2.8
Mixed scheme				
PBE0	1.2	8.9	4.4	3.3
HSE	1.2	8.9	4.6	3.2
Expt.	1.2	8.9	4.4	3.4

deviations up to several electron volts might persist when compared to experiment (cf. Table IV).[29] In Ref. 29, it was argued that this discrepancy mainly results from the persisting deficiency of hybrid functionals in describing band gaps. Indeed, a mixed scheme which yields optimal band gaps for both interface components showed excellent agreement with experiment for a set of three different interfaces.[29] This scheme consists in determining the bulk band edges through a PBE0-like calculation in which the fraction α is tuned to give the experimental band gap. The band structure are then aligned through the potential lineup, which does not sensitively depend on α.[29] Table IV shows that in the case of the Si-SiO_2 interface a good agreement between theory and experiment is also achieved when using HSE-like functionals rather than PBE0-like ones. Note that this agreement directly stems from the close positions of the valence-band edges found with α-tuned PBE0-like and HSE-like functionals (Table III), and is therefore expected to carry more general validity.

V. RATIONALE

In this section, we provide a rationale for the material-independent relationships between total-energy differences and generalized Kohn-Sham eigenvalues obtained with the PBE0, HSE, and sPBE0 functionals.

A. Total energies

We first focus on properties such as ionization potentials or charge transition levels, which can be expressed in terms of total-energy differences. For such quantities, we observed (i) a very good agreement between PBE0 and HSE and (ii) a material-independent shift of ~0.4 eV between sPBE0 and PBE0 (or equivalently HSE).

The good agreement between total-energy differences in PBE0 and HSE has already amply been demonstrated in the literature.[8] This applies in a straightforward way to ionization potentials of molecular systems. Following Ref. 22, this

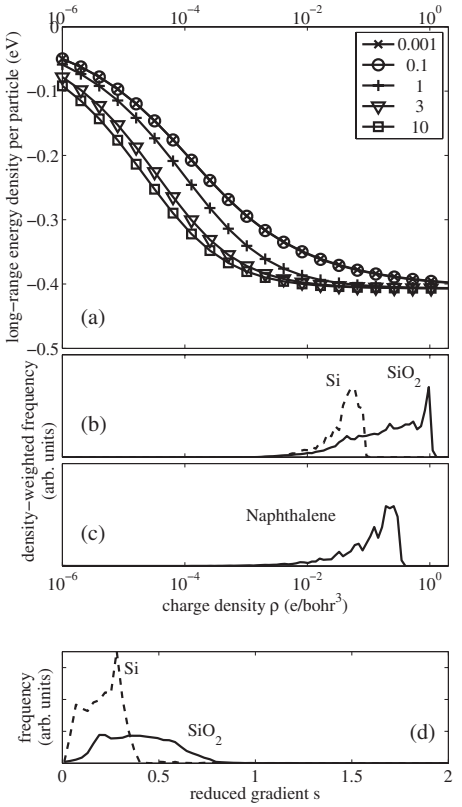

FIG. 6. (a) Long-range exchange energy density per electron $E_x^{\mathrm{PBE,LR}}$ as a function of density ρ and for different values of the reduced gradient s (from Ref. 8). The ω parameter is fixed at the HSE value of 0.106 bohr^{-1} (Ref. 33). Also shown are the density-weighted distributions of charge densities for (b) SiO_2 (solid) and Si (dashed) and (c) naphthalene, and (d) the distribution of reduced gradients s for SiO_2 (solid) and Si (dashed).

argument naturally extends to charge transition levels of atomic-size defects provided they are referred to the average electrostatic potential. This explains the close agreement in Fig. 1 between PBE0 and HSE charge transition levels.

The shift of ~0.4 eV found for sPBE0 calculations necessarily results from the missing long-range exchange. Whether nonlocal as in PBE0 or local as in HSE, this missing part appears to produce equivalent effects supporting the accuracy of the HSE functional.[8] For simplicity, we focus in this section on the local expression for long-range exchange,

$$E_x^{\mathrm{PBE,LR}}(\omega) = \int \epsilon_x^{\mathrm{PBE,LR}}[\rho(\mathbf{r}), s, \omega]\rho(\mathbf{r})d\mathbf{r}, \tag{6}$$

where the long-range energy density per electron $\epsilon_x^{\mathrm{PBE,LR}}$ is defined as the difference between the PBE exchange energy density and the short-range PBE exchange energy density, introduced in Ref. 8: $\epsilon_x^{\mathrm{PBE}} - \epsilon_x^{\mathrm{PBE,SR}}$. The energy density $\epsilon_x^{\mathrm{PBE,LR}}$ is plotted in Fig. 6 as a function of both the density ρ and the reduced gradient $s = |\nabla\rho|/(2k_F\rho)$, where $k_F = (3\pi^2\rho)^{1/3}$. We note that for all considered values of the reduced gradient, the energy density $\epsilon_x^{\mathrm{PBE,LR}}$ flattens out at large charge densities assuming a value of about −0.4 eV per electron. The plateau sets in at lower charge density values when the reduced gradient s increases.

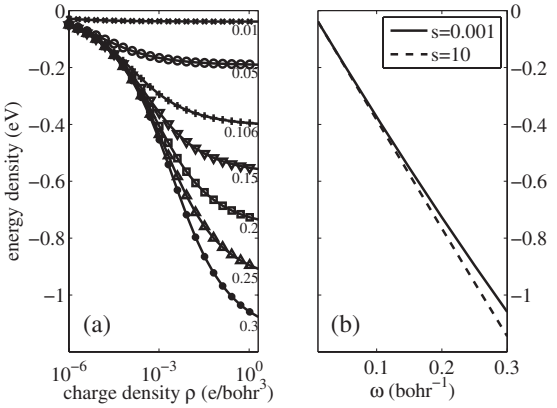

FIG. 7. (a) Long-range exchange energy density per electron $\epsilon_x^{\mathrm{PBE,LR}}$ as given in Ref. 8 (a) as a function of density ρ for different values of ω ranging between 0.01 and 0.3 and for $s=0.001$, and (b) as a function of ω for two values of s and at a fixed density $\rho = 1\ e/\mathrm{bohr}^3$.

The range of interest for real systems is $\rho > 2.5 \times 10^{-4}$ a.u. and $0 < s < 3$ (Ref. 31). Furthermore, we note that the integrand in Eq. (6) is density weighted, thus effectively reducing the significance of low values of the charge density. From these considerations, it appears that for any real system the long-range exchange energy per electron is expected to give a value ranging in between −0.35 and −0.40 eV. For illustration, we also show in Fig. 6 distributions of charge densities and of reduced gradients, corresponding to SiO_2, Si, and naphtalene. These distributions clearly demonstrate that the integrand has a predominant weight for energy densities falling in the plateau region.

When the energy density assumes a nearly constant value, the total long-range exchange energy can be approximated as

$$E_x^{\mathrm{PBE,LR}} = \int \epsilon_x^{\mathrm{LR}}\rho(\mathbf{r})d\mathbf{r} \approx N_e\epsilon_x^{\mathrm{LR}}, \tag{7}$$

where N_e is the total number of electrons in the system and $\epsilon_x^{\mathrm{LR}} \approx -0.4$ eV, nearly independent of the considered electronic system. This contribution accounts for the difference between the total energy in sPBE0 and those obtained in PBE0 or HSE, and can be used to correct sPBE0 calculations *a posteriori*. In the ionization potential calculations for the molecules in Sec. III A, a total-energy difference is considered between systems with N and $N-1$ electrons. Hence, the missing long-range exchange energy in sPBE0 explains the observed shift of ~0.4 eV in the ionization potentials involving a transition of a single electron. The same reasoning also applies to the charge transition levels in Fig. 1.

It is important to point out that the value $\epsilon_x^{\mathrm{LR}} \approx -0.4$ eV depends on the adopted values for the parameters α and ω. While the dependence on α is simply linear, the effect of the screening parameter ω is less trivial. In Fig. 7(a), the dependence of ϵ_x^{LR} on the charge density is illustrated for various values of ω. The onset of the plateau depends on ω, and moves to larger charge densities as ω increases. The plateau

TABLE V. Valence-band edge shifts (ΔE_v), conduction-band edge shifts (ΔE_c), and band-gap shifts (ΔE_g) of HSE and PBE0 with respect to sPBE0. The band structures of calculations with different functionals are aligned through the average electrostatic potential. All energies are in electron volt.

	HSE			PBE0		
	ΔE_v	ΔE_c	ΔE_g	ΔE_v	ΔE_c	ΔE_g
Si	−0.39	−0.37	0.02	−0.72	−0.05	0.67
SiC	−0.40	−0.38	0.01	−0.79	−0.01	0.78
HfO_2	−0.40	−0.38	0.02	−0.80	−0.01	0.79
SiO_2	−0.40	−0.37	0.03	−0.80	−0.01	0.80

value of ϵ_x^{LR} depends almost linearly on ω, as shown in Fig. 7(b). However, the property of achieving a constant material-independent contribution for ϵ_x^{LR} depends on the extent of realistic charge density distributions. For values of ω up to 0.106 bohr^{-1}, i.e., the value used in the HSE functional,[33] these electronic distributions almost completely locate in the plateau region but for larger values of ω, this property progressively deteriorates. Thus it appears that the value of 0.106 bohr^{-1} for ω is about the largest one compatible with a constant material-independent ϵ_x^{LR}. In other words, the screening length in HSE is the smallest one for which the long-range exchange energy density is essentially still material independent. In HSE, the latter is treated locally while the material-dependent short-range exchange is treated by a close approximation of the nonlocal exact expression.

The discussion in this section is based on charge densities which were obtained in the pseudopotential approximation. When the charge density in all-electron approaches includes that of the core electrons, higher densities (and higher gradients) are expected in the core regions. Consideration of such high densities pushes ϵ_x^{LR} even further into the plateau region, reenforcing the constant nature of the average long-range exchange energy density.

B. Generalized Kohn-Sham eigenvalues

Table V collects the shifts of the generalized Kohn-Sham eigenvalues for HSE and PBE0 with respect to sPBE0. The shifts reported in this table show trends which appear to be material independent. In the comparison between HSE and sPBE0, we observe a systematic downward shift by ~0.4 eV of the band structure. The comparison between PBE0 and sPBE0 suggests a closure of the band gap by ~0.8 eV by the sole displacement of the occupied states. For the materials studied, the deviations from these general trends are within only 0.03 eV, except for silicon for which the largest calculated deviation is 0.13 eV. In the following, we provide a rationale for these features.

The relation between the band structures of sPBE0 and HSE follows from the analysis in the previous section. The effect of the long-range PBE exchange on the eigenvalues can be obtained from the functional derivative,

$$v_x^{PBE,LR} = \frac{\partial E_x^{PBE,LR}}{\partial \rho}. \tag{8}$$

In the regime in which the long-range exchange density is constant, this results in a constant shift of the local potential. Hence, both occupied and unoccupied states in HSE are shifted downward with respect to their sPBE0 values.

To address the comparison between the generalized Kohn-Sham eigenvalues of PBE0 and sPBE0, we describe the eigenvalue shifts using perturbation theory, $\Delta\varepsilon_n = \langle n|\Delta\hat{v}_x^{PBE,LR}|n\rangle$, where $\Delta\hat{v}_x^{PBE,LR}$ corresponds to the long-range part of the exact nonlocal exchange, which determines the difference between PBE0 and sPBE0.

In a plane-wave basis set, the shift in the eigenvalues reads[58]

$$\Delta\varepsilon_n(\mathbf{k}) = \sum_{\mathbf{G},\mathbf{G}'} c_n^*(\mathbf{G}+\mathbf{k})\langle \mathbf{G}+\mathbf{k}|\Delta\hat{v}_x^{PBE,LR}|\mathbf{G}'+\mathbf{k}\rangle c_n(\mathbf{G}'+\mathbf{k}), \tag{9}$$

where the c_n correspond to the coefficients of the wave functions in the plane-wave representation and where the matrix element of the exchange potential is given by

$$\langle \mathbf{G}+\mathbf{k}|\Delta\hat{v}_x^{PBE,LR}|\mathbf{G}'+\mathbf{k}\rangle = -\frac{\alpha}{2\pi^2}\sum_m \int c_m^*(\mathbf{G}'+\mathbf{Q})c_m(\mathbf{G}+\mathbf{Q})\frac{e^{-|\mathbf{k}-\mathbf{Q}|^2/(4\omega^2)}}{|\mathbf{k}-\mathbf{Q}|^2}d\mathbf{Q}, \tag{10}$$

where the sum over m corresponds to a sum over occupied states and the integration over $\mathbf{Q}$ is over the whole of reciprocal space. The Coulomb-type kernel decays exponentially as $|\mathbf{k}-\mathbf{Q}|$ increases and the decay length is set by ω. We have seen in the previous section that the HSE value for ω is chosen small enough to ensure that the long-range exchange remains material independent. Hence, we assume that ω is so small that contributions only result from $\mathbf{Q}$ very close to $\mathbf{k}$ and that the following approximation holds:

$$c_m(\mathbf{G}+\mathbf{Q}) \approx c_m(\mathbf{G}+\mathbf{k}). \tag{11}$$

The remaining integral over $\mathbf{Q}$ in Eq. (10) can be carried out analytically for any $\mathbf{k}$,

$$\frac{\alpha}{2\pi^2}\int \frac{e^{-|\mathbf{k}-\mathbf{Q}|^2/(4\omega^2)}}{|\mathbf{k}-\mathbf{Q}|^2}d\mathbf{Q} = \frac{2\alpha\omega}{\sqrt{\pi}}. \tag{12}$$

For α=25% and ω=0.106 bohr^{-1}, this gives the value of 0.814 eV. The expression in Eq. (9) resulting from the summations over $\mathbf{G}$ and $\mathbf{G}'$ then simplifies because of the orthonormality of the wave functions,

$$\sum_{\mathbf{G},\mathbf{G}',m} c_n^*(\mathbf{G}+\mathbf{k})c_m(\mathbf{G}+\mathbf{k})c_m^*(\mathbf{G}'+\mathbf{k})c_n(\mathbf{G}'+\mathbf{k}) = \sum_m \delta_{nm}^2. \tag{13}$$

Since the sum over m only concerns occupied states, this factor vanishes for unoccupied states and is equal to 1 for occupied states. These considerations provide a rationale for the relative positions of PBE0 and sPBE0 eigenvalues.

We note that the above derivation relies on the validity of the approximation in Eq. (11) when the distance in reciprocal space between **Q** and **k** varies within a range determined by the inverse screening length ω. This approximation is expected to deteriorate when the wave-function coefficients undergo strong variations for **k** varying in reciprocal space. This is more likely to occur for small band-gap materials and explains that the largest deviation from the general trend is observed for silicon in Table V.

The shift of ~0.8 eV between the eigenvalues of the occupied states in PBE0 and sPBE0 is not unrelated to the shift of ~0.4 eV per electron between the PBE0 and sPBE0 total energies discussed in Sec. V A. Indeed, the total exchange energy can be expressed as $E_x=\frac{1}{2}\Sigma_n^{\mathrm{occ}}\langle\psi_n|\hat{v}_x|\psi_n\rangle$, where the factor 1/2 arises from the double counting of the interactions. Note also that the shift of the defect levels by +0.4 eV when going from PBE0 to sPBE0 is consistent with Slater's transition-state theorem,[59]

$$E_{N-1}-E_N=-\varepsilon_n(1/2)\approx-\frac{\varepsilon_n(0)+\varepsilon_n(1)}{2}, \qquad (14)$$

where $\varepsilon_n(f)$ specifies the generalized Kohn-Sham eigenvalue at occupation f. Indeed, $\Delta(E_{N-1}-E_N)\cong 0.4$ eV, $\Delta[\varepsilon_n(0)]\cong 0$, and $\Delta[\varepsilon_n(1)]\cong 0.8$ eV.

VI. CONCLUSIONS

We have carried out a comparative study involving the semilocal density functional PBE and three PBE-based hybrid functionals, including PBE0, HSE, and sPBE0. The three hybrid functionals differ by the way the long-range exchange energy is treated, namely, it is included at the exact nonlocal level in PBE0, by a local expression in HSE, and is fully neglected in sPBE0. The comparison focused on both total energies and generalized Kohn-Sham eigenvalues. Physical quantities concerned by our study are, for instance, ionization potentials, charge transition levels of defects, band gaps, band offsets at interfaces, and positions of defects levels within band gaps. As the hybrid functionals considered in this work are becoming increasingly popular to determine these quantities, this investigation provides clear guidance for comparing results achieved with different functionals. An additional benefit achieved in this study is a deeper understanding of the role of both local and nonlocal long-range exchange.

In this work, we focused on effects resulting from different descriptions of the exchange interaction in hybrid functionals. For this purpose, we performed all calculations with the structural models relaxed at the PBE level. It is thus understood that all the effects identified here do not include relaxation effects. This limitation does not appear to be a critical one since structural improvements achieved through the use of hybrid functionals are generally minor, except when driven by important modifications of the electronic structure itself.

The main results achieved in this work are schematically illustrated in Fig. 8. The figure shows the relative behavior of band edges and defect levels when calculations with different hybrid functionals are aligned through the average electrostatic potential. While the band edges correspond to generalized Kohn-Sham eigenvalues, the defect level is representative of quantities determined through total energy differences. In fact, the illustrated relationships apply without modification to HOMO/LUMO levels and to ionization potentials in the case of finite molecular systems.

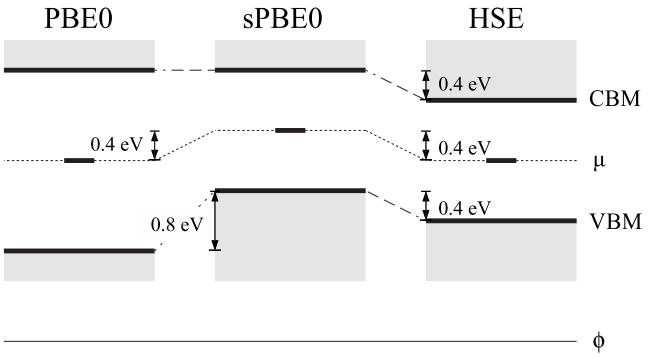

FIG. 8. Schematic representation of relative position of valence-band (VBM) and conduction-band (CBM) edges as obtained from the generalized Kohn-Sham eigenvalues with different hybrid functionals. A defect charge transition level μ as obtained through differences of total energies is also represented. The different electronic structures are aligned through the average electrostatic potential ϕ. Note that the indicated shifts of ~0.4 eV and ~0.8 eV are material-independent.

Quantities derived from total energies, including both ionization potentials of molecules and charge transition levels of defects, are found to be very similar in PBE0 and in HSE (cf. Fig. 8), consistent with other comparisons in the literature.[43,60] When long-range exchange is fully omitted as in sPBE0, we found the total energies to increase by about 0.4 eV per electron compared to PBE0 or HSE.

The generalized Kohn-Sham eigenvalues obtained with the three hybrid functionals also show characteristic shifts (cf. Fig. 8). With respect to PBE0, the band gap in sPBE0 closes by ~0.8 eV, and results from an upward displacement of all the occupied states. Going from sPBE0 to HSE, all the eigenvalues shift down by ~0.4 eV. Hence, the HSE eigenvalues are obtained from the PBE0 ones by an upwards shift of the occupied levels by ~0.4 eV and a downward shift of the unoccupied levels by the same amount. It is important to note that all these shifts are to a large extent independent of the system studied, allowing for simple comparisons between calculations performed within this set of hybrid functionals.

The scheme in Fig. 8 can also be used to compare the position of defect levels in the band gap when referenced with respect to the valence-band maxima. Accounting for the relative shifts of the band edges and of the defect level, one finds that the defect level in PBE0 lies 0.4 eV higher with respect to the valence-band edge than in sPBE0 and in HSE. This shift needs to be accounted for when comparing defect levels in HSE and PBE0 calculations. At variance, not only the size of the band gap but also the location of the defect level within the band gap is identical in sPBE0 and in HSE, despite their different situation with respect to the average electrostatic potential. This implies, for instance, that earlier

defect-level calculations in sPBE0 (Ref. 20) can just as well be thought as obtained with HSE.

The band offsets at interfaces calculated with various hybrid functionals were also addressed in this work. All the hybrid functionals considered reproduce interface dipoles in an equivalent way. Hence, differences in band offsets only result from shifts of the band edges when going from one hybrid functional to another (cf. Fig. 8). These shifts have been found to be independent of material, and thus are the same for both interface components. Combined with the equivalent interface dipoles, one concludes that the band offsets calculated with any hybrid functional considered are nearly identical.

The material-independent nature of the shifts between total energies and eigenvalues obtained with the various functionals is here not only empirically observed for specific case studies but also supported by general considerations. These considerations point out that the screening parameter, $\omega = 0.106$ bohr^{-1}, introduced in HSE, is such that the resulting long-range exchange energy can well be approximated by a fixed material-independent energy per electron. This observation underlies all the shifts in Fig. 8. Furthermore, the constant nature of the long-range nonlocal exchange energy supports its replacement by a local expression as done in HSE, shedding light on the overall good agreement between total energies determined in PBE0 and HSE.

Finally, we considered differences between PBE0-like and HSE-like functionals that might arise when adhering to the common practice of tuning α for reproducing the experimental band gap. This practice is, in principle, not equivalent when applied to PBE0 or HSE. In PBE0, the band-edge shifts are governed by exact nonlocal exchange, which generally results in unequal shifts of the conduction and valence bands. At variance, in HSE, part of the band-edge shifts is accounted for by constant shifts that act symmetrically on valence- and conduction-band edges. Nevertheless, our investigation shows that the resulting differences are very small, finding differences in band-edge levels of only ~ 0.2 eV in the worst case. This result implies that, when the band gap is tuned, PBE0 and HSE yield nearly identical results for defect level positions in the band gap and for band offsets at interfaces.

ACKNOWLEDGMENTS

We thank Gustavo E. Scuseria for providing us with a copy of Jochen Heyd's thesis where subroutines specific to HSE can be found (Ref. 41). We also thank Audrius Alkauskas for providing us with defect structures. Useful discussions are acknowledged with C. G. Van de Walle and members of his research group. Financial support is acknowledged from the Swiss National Science Foundation under Grant No. 200020-119733/1. Calculations were performed at computer facilities at EPFL and CSCS.

*hannu.komsa@epfl.ch

[1] A. D. Becke, J. Chem. Phys. **98**, 1372 (1993).
[2] S. Kümmel and L. Kronik, Rev. Mod. Phys. **80**, 3 (2008).
[3] L. A. Curtiss, P. C. Redfern, K. Raghavachari, and J. A. Pople, J. Chem. Phys. **106**, 1063 (1997); **109**, 42 (1998).
[4] A. Dal Corso, A. Pasquarello, A. Baldereschi, and R. Car, Phys. Rev. B **53**, 1180 (1996).
[5] I.-H. Lee and R. M. Martin, Phys. Rev. B **56**, 7197 (1997).
[6] M. Ernzerhof and G. E. Scuseria, J. Chem. Phys. **110**, 5029 (1999).
[7] C. Adamo and V. Barone, J. Chem. Phys. **110**, 6158 (1999).
[8] J. Heyd, G. E. Scuseria, and M. Ernzerhof, J. Chem. Phys. **118**, 8207 (2003).
[9] J. Paier, M. Marsman, K. Hummer, G. Kresse, I. C. Gerber, and J. G. Ángyán, J. Chem. Phys. **125**, 249901 (2006).
[10] E. R. Batista, J. Heyd, R. G. Hennig, B. P. Uberuaga, R. L. Martin, G. E. Scuseria, C. J. Umrigar, and J. W. Wilkins, Phys. Rev. B **74**, 121102(R) (2006).
[11] J. Muscat, A. Wander, and N. M. Harrison, Chem. Phys. Lett. **342**, 397 (2001).
[12] J. Heyd, J. E. Peralta, G. E. Scuseria, and R. L. Martin, J. Chem. Phys. **123**, 174101 (2005).
[13] J. Paier, M. Marsman, K. Hummer, G. Kresse, I. C. Gerber, and J. G. Ángyán, J. Chem. Phys. **124**, 154709 (2006).
[14] E. N. Brothers, A. F. Izmaylov, J. O. Normand, V. Barone, and G. E. Scuseria, J. Chem. Phys. **129**, 011102 (2008).
[15] C. Adamo, G. E. Scuseria, and V. Barone, J. Chem. Phys. **111**, 2889 (1999).
[16] J. Lento and R. M. Nieminen, J. Phys.: Condens. Matter **15**, 4387 (2003).
[17] K. Xiong, J. Robertson, M. C. Gibson, and S. J. Clark, Appl. Phys. Lett. **87**, 183505 (2005).
[18] J. M. Knaup, P. Deák, Th. Frauenheim, A. Gali, Z. Hajnal, and W. J. Choyke, Phys. Rev. B **72**, 115323 (2005).
[19] J. L. Gavartin, D. M. Ramo, A. L. Shluger, G. Bersuker, and B. H. Lee, Appl. Phys. Lett. **89**, 082908 (2006).
[20] P. Broqvist and A. Pasquarello, Appl. Phys. Lett. **89**, 262904 (2006).
[21] P. Broqvist and A. Pasquarello, Appl. Phys. Lett. **90**, 082907 (2007).
[22] A. Alkauskas, P. Broqvist, and A. Pasquarello, Phys. Rev. Lett. **101**, 046405 (2008).
[23] A. Alkauskas, P. Broqvist, and A. Pasquarello, Phys. Rev. B **78**, 161305(R) (2008).
[24] P. Broqvist, A. Alkauskas, and A. Pasquarello, Phys. Rev. B **78**, 075203 (2008).
[25] F. Oba, A. Togo, I. Tanaka, J. Paier, and G. Kresse, Phys. Rev. B **77**, 245202 (2008).
[26] A. Carvalho, A. Alkauskas, A. Pasquarello, A. K. Tagantsev, and N. Setter, Phys. Rev. B **80**, 195205 (2009).
[27] J. B. Varley, A. Janotti, A. K. Singh, and C. G. Van de Walle, Phys. Rev. B **79**, 245206 (2009).
[28] M.-H. Du and S. B. Zhang, Phys. Rev. B **80**, 115217 (2009).
[29] A. Alkauskas, P. Broqvist, F. Devynck, and A. Pasquarello, Phys. Rev. Lett. **101**, 106802 (2008).
[30] F. Devynck, F. Giustino, P. Broqvist, and A. Pasquarello, Phys.

Rev. B **76**, 075351 (2007); the corrected version of Table III is given in F. Devynck, Ph.D. thesis, Ecole Polytechnique Fédérale de Lausanne, 2008.
[31] J. P. Perdew, K. Burke, and M. Ernzerhof, Phys. Rev. Lett. **77**, 3865 (1996).
[32] J. P. Perdew, M. Ernzerhof, and K. Burke, J. Chem. Phys. **105**, 9982 (1996).
[33] J. Heyd, G. E. Scuseria, and M. Ernzerhof, J. Chem. Phys. **124**, 219906 (2006).
[34] D. M. Bylander and L. Kleinman, Phys. Rev. B **41**, 7868 (1990).
[35] T. Todorova, A. P. Seitsonen, J. Hutter, I.-F. W. Kuo, and C. J. Mundy, J. Phys. Chem. B **110**, 3685 (2006).
[36] C. G. Van de Walle and J. Neugebauer, J. Appl. Phys. **95**, 3851 (2004).
[37] G. Makov and M. C. Payne, Phys. Rev. B **51**, 4014 (1995).
[38] P. Broqvist, A. Alkauskas, and A. Pasquarello, Phys. Rev. B **80**, 085114 (2009).
[39] P. Giannozzi, S. Baroni, N. Bonini, M. Calandra, R. Car, C. Cavazzoni, D. Ceresoli, G. L. Chiarotti, M. Cococcioni, I. Dabo, A. Dal Corso, S. de Gironcoli, S. Fabris, G. Fratesi, R. Gebauer, U. Gerstmann, C. Gougoussis, A. Kokalj, M. Lazzeri, L. Martin-Samos, N. Marzari, F. Mauri, R. Mazzarello, S. Paolini, A. Pasquarello, L. Paulatto, C. Sbraccia, S. Scandolo, G. Sclauzero, A. P. Seitsonen, A. Smogunov, P. Umari, and R. M. Wentzcovitch, J. Phys.: Condens. Matter **21**, 395502 (2009).
[40] CPMD, http://www.cpmd.org/, Copyright IBM Corp. 1990–2008, Copyright MPI für Festkörperforschung Stuttgart 1997–2001.
[41] The original HSE subroutines in Jochen Heyd's thesis were kindly provided to us by G. E. Scuseria.
[42] M. Ernzerhof and J. P. Perdew, J. Chem. Phys. **109**, 3313 (1998).
[43] J. Paier, R. Hirschl, M. Marsman, and G. Kresse, J. Chem. Phys. **122**, 234102 (2005).
[44] *NIST Chemistry WebBook*, NIST Standard Reference Database No. 69, edited by P. J. Linstrom and W. G. Mallard (National Institute of Standards and Technology, Gaithersburg, MD, 2005), p. 20899.
[45] A. Seidl, A. Görling, P. Vogl, J. A. Majewski, and M. Levy, Phys. Rev. B **53**, 3764 (1996).
[46] A. Alkauskas and A. Pasquarello, Physica B **401-402**, 670 (2007).
[47] W. M. Yim and R. J. Paff, J. Appl. Phys. **45**, 1456 (1974).
[48] Y. S. Park, in *SiC Materials and Devices*, edited by R. K. Willardson and E. R. Weber (Academic Press, New York, 1998), Vol. 52.
[49] J. Adam and M. D. Rogers, Acta Crystallogr. **12**, 951 (1959).
[50] J. C. Brice, J. Mater. Sci. **15**, 161 (1980).
[51] A. V. Krukau, O. A. Vydrov, A. F. Izmaylov, and G. E. Scuseria, J. Chem. Phys. **125**, 224106 (2006).
[52] C. G. Van de Walle and R. M. Martin, Phys. Rev. B **34**, 5621 (1986).
[53] F. Giustino and A. Pasquarello, Phys. Rev. Lett. **95**, 187402 (2005); A. Bongiorno, A. Pasquarello, M. S. Hybertsen, and L. C. Feldman, *ibid.* **90**, 186101 (2003); A. Bongiorno and A. Pasquarello, Appl. Phys. Lett. **83**, 1417 (2003).
[54] J. Sarnthein, A. Pasquarello, and R. Car, Phys. Rev. Lett. **74**, 4682 (1995); Phys. Rev. B **52**, 12690 (1995).
[55] J. L. Lyons, A. Janotti, and C. G. Van de Walle, Phys. Rev. B **80**, 205113 (2009).
[56] A. Alkauskas, P. Broqvist, and A. Pasquarello (unpublished).
[57] F. J. Himpsel, F. R. McFeely, A. Taleb-Ibrahimi, J. A. Yarmoff, and G. Hollinger, Phys. Rev. B **38**, 6084 (1988); J. W. Keister, J. E. Rowe, J. J. Kolodziej, H. Niimi, T. E. Madey, and G. Lucovsky, J. Vac. Sci. Technol. B **17**, 1831 (1999).
[58] An alternative but equivalent approach consists in analyzing $\Delta\varepsilon_n$ in real space by keeping only the first term in the series expansion of the kernel $\mathrm{erf}(\omega r)/r$. This term is independent of r.
[59] J. C. Slater, Adv. Quantum Chem. **6**, 1 (1972); J. F. Janak, Phys. Rev. B **18**, 7165 (1978).
[60] J. Heyd and G. E. Scuseria, J. Chem. Phys. **121**, 1187 (2004).